Report

Neuron

Neuroligin-4 Regulates Excitatory Synaptic Transmission in Human Neurons

Highlights

- In human brain, the synaptic protein NLGN4 is primarily expressed in cerebral cortex
- Unlike in mouse, human NLGN4 protein preferentially localizes to glutamatergic synapses
- NLGN4 gain of function induces an excitatory synaptic phenotype in human neurons
- R704C increases excitatory synapse density, synapse transmission, and AMPAR affinity

Authors

Samuele G. Marro, Soham Chanda, Nan Yang, ..., M. Yashar S. Kalani, Thomas C. Südhof, Marius Wernig

Correspondence

tcs1@stanford.edu (T.C.S.), wernig@stanford.edu (M.W.)

In Brief

Disruption of the gene Neuroligin-4 is rare in autism but has almost complete penetrance. Neuroligin-4 is unique to human. Marro et al. use human neurons derived from embryonic stem cells to describe a new role for Neuroligin-4 in excitatory synapses.

Marro et al., 2019, Neuron *103*, 617–626
August 21, 2019
https://doi.org/10.1016/j.neuron.2019.05.043

CellPress

Neuron
Report

Neuroligin-4 Regulates Excitatory Synaptic Transmission in Human Neurons

Samuele G. Marro,[1,2,6] Soham Chanda,[1,2,4,6,7] Nan Yang,[1,2,8] Justyna A. Janas,[1,2] Giulio Valperga,[1,2] Justin Trotter,[4,5] Bo Zhou,[1,2,4] Sean Merrill,[4,5] Issa Yousif,[1,2] Hannah Shelby,[1,2] Hannes Vogel,[1] M. Yashar S. Kalani,[3] Thomas C. Südhof,[4,5,*] and Marius Wernig[1,2,9,*]

[1]Department of Pathology, Stanford University School of Medicine, Stanford, CA 94305, USA
[2]Institute for Stem Cell Biology and Regenerative Medicine, Stanford University School of Medicine, Stanford, CA 94305, USA
[3]Departments of Neurosurgery and Neuroscience, University of Virginia School of Medicine, Charlottesville, VA 22908, USA
[4]Department of Molecular and Cellular Physiology, Stanford University School of Medicine, Stanford, CA 94305, USA
[5]Howard Hughes Medical Institute, Stanford University School of Medicine, Stanford, CA 94305, USA
[6]These authors contributed equally
[7]Present address: Department of Biochemistry and Molecular Biology, Colorado State University, Fort Collins, CO 80523, USA
[8]Present address: Department of Neuroscience, Black Family Stem Cell Institute, Friedman Brain Institute, Icahn School of Medicine at Mount Sinai, New York, NY 10029, USA
[9]Lead Contact
*Correspondence: tcs1@stanford.edu (T.C.S.), wernig@stanford.edu (M.W.)
https://doi.org/10.1016/j.neuron.2019.05.043

SUMMARY

The autism-associated synaptic-adhesion gene *Neuroligin-4* (*NLGN4*) is poorly conserved evolutionarily, limiting conclusions from Nlgn4 mouse models for human cells. Here, we show that the cellular and subcellular expression of human and murine Neuroligin-4 differ, with human Neuroligin-4 primarily expressed in cerebral cortex and localized to excitatory synapses. Overexpression of NLGN4 in human embryonic stem cell-derived neurons resulted in an increase in excitatory synapse numbers but a remarkable decrease in synaptic strength. Human neurons carrying the syndromic autism mutation NLGN4-R704C also formed more excitatory synapses but with increased functional synaptic transmission due to a postsynaptic mechanism, while genetic loss of NLGN4 did not significantly affect synapses in the human neurons analyzed. Thus, the NLGN4-R704C mutation represents a change-of-function mutation. Our work reveals contrasting roles of NLGN4 in human and mouse neurons, suggesting that human evolution has impacted even fundamental cell biological processes generally assumed to be highly conserved.

INTRODUCTION

Neuroligins are postsynaptic adhesion molecules that control the maturation and function of synapses in a surprisingly diverse fashion. In humans, there are four neuroligin genes: the autosomal *NLGN1* and *NLGN2* genes and the X chromosomal *NLGN3* and *NLGN4* genes. Point mutations and CNVs in neuroligin genes were observed in patients with familial autism spectrum disorders (ASD) (Südhof, 2008, 2017). Although most ASD cases are non-syndromic, they are still largely associated with genetic factors (Beaudet, 2007) that are characterized by extreme genetic heterogeneity, possibly involving hundreds of genes with individually low penetrance (Iossifov et al., 2014; Neale et al., 2012; O'Roak et al., 2012; Sanders et al., 2012). Neuroligin mutations are among the few genes that have high penetrance, establishing a clear causative connection with ASD. Among neuroligins, NLGN4 is most frequently found to be mutated, and more than 50 distinct NLGN4 mutations have been described in ASD patients with a nearly 100% penetrant phenotype (Chocholska et al., 2006; Jamain et al., 2003; Laumonnier et al., 2004; Lawson-Yuen et al., 2008; Macarov et al., 2007; Marshall et al., 2008; Pampanos et al., 2009; Talebizadeh et al., 2006; Yan et al., 2005). Only a single mutation affected specifically the cytoplasmic sequences of NLGN4, the R704C substitution (Yan et al., 2005). This mutation targets a residue conserved in all neuroligins and when introduced in Nlgn3 induced a strong glutamatergic synaptic transmission phenotype (Chanda et al., 2013; Etherton et al., 2011; Zhang et al., 2017). Despite the need to understand NLGN4's function, little is known about NLGN4 compared to the other neuroligins. No Nlgn4 homolog was identified in *Rattus norvegicus*, and the mouse ortholog (called *Nlgn4-like*) is poorly conserved, is not located on the X chromosome, and is to this day not included in the assembled mouse genome sequence (Bolliger et al., 2008). Moreover, mouse *Nlgn4* is expressed only at low levels (Varoqueaux et al., 2006) and the Nlgn4 protein was reported to be restricted to inhibitory glycinergic synapses in brain stem, retina, and spinal cord within the central nervous system (CNS) (Hoon et al., 2011). *Nlgn4* KO mice showed behavioral abnormalities (Delattre et al., 2013; Hammer et al., 2015; Hoon et al., 2011; Ju et al., 2014; Unichenko et al., 2018; Zhang et al., 2018a). On the other hand, overexpression of human NLGN4 in mouse hippocampal neurons resulted in a complex phenotype in excitatory but not inhibitory synapses (Chanda et al., 2016; Unichenko et al., 2018; Zhang et al., 2009). To complicate things further, human NLGN4 expression in rat hippocampal slice cultures was shown to cause a different excitatory synapse

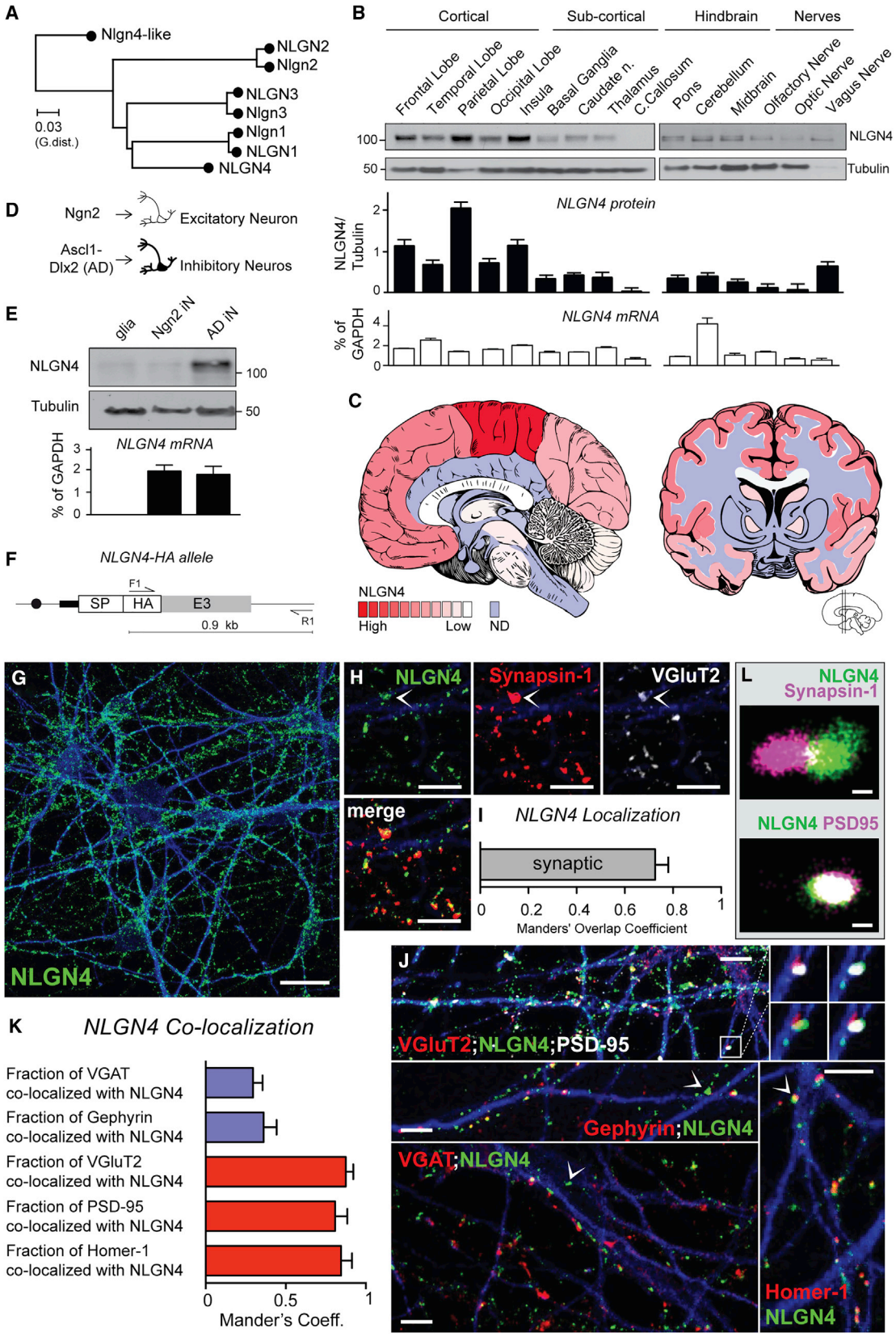

(legend on next page)

phenotype (Bemben et al., 2015). These incoherent results derived from various animal models are difficult to interpret and raise questions of relevance for humans. Therefore, we here investigated the function of human NLGN4 and the R704C mutation in human neurons.

RESULTS

Human NLGN4 Protein Is Divergent from Its Closest Mouse Ortholog, Primarily Expressed in Cortex, and Preferentially Localizes to Excitatory Postsynaptic Compartments

The human NLGN4 has a higher amino acid homology to mouse Nlgn1, 2, and 3 than to Nlgn4-like (Figure 1A). For example, the C-terminal domain is more similar to mouse Nlgn1 than Nlgn4-like (Figure S1A). Nevertheless, Nlgn4 has been studied exclusively in rodents. To investigate the role of human NLGN4, we assessed its expression pattern in the normal human brain. We used an antibody that recognizes a specific NLGN4 band on immunoblot of non-fixed tissue (Figure S1B). Unfortunately, the antibody did not produce a specific band on fixed tissue or in immunofluorescence staining. We therefore obtained flash frozen tissue samples from various areas of the CNS after rapid autopsy of two donors without neurological disorders. NLGN4 protein could be detected with the highest levels in all cortical samples and substantially lower expression in other areas (Figures 1B, 1C, and S1C). This finding was surprising because the localization of mouse Nlgn4 had been primarily observed in the mouse brainstem, retina, and spinal cord (Hoon et al., 2011). As shown for other neuroligins, NLGN4 protein levels did not correlate with the mRNA levels (Bolliger et al., 2008; Varoqueaux et al., 2006). Neuroligins are expressed in glia in addition to neurons (Gilbert et al., 2001; Zhang et al., 2014). To verify expression of NLGN4 in human neurons, we generated pure cultures of excitatory and inhibitory neurons derived from human embryonic stem cells (ESCs). ESCs were differentiated into excitatory neurons (iN cells) with dorsal forebrain characteristics by expressing the transcription factor Ngn2 (Ngn2 iN cells) and to inhibitory neurons with characteristics of ventral forebrain by expressing Ascl1 and Dlx2 (AD iN cells) (Figure 1D; Yang et al., 2017; Zhang et al., 2013). Lysates from AD iN cells contained NLGN4 protein at levels comparable to brain, whereas Ngn2 iN cells lacked NLGN4 protein even though expressed similar amounts of mRNA (Figure 1E).

We then aimed to investigate the subcellular localization of NLGN4, but the lack of antibodies made direct labeling impossible. Thus, we knocked-in the human influenza hemagglutinin (HA) into the human *NLGN4* gene (C-terminal to the extracellular sequence) in ESCs (Khan et al., 2011; Pak et al., 2015; Patzke et al., 2015; Russell and Hirata, 1998; Yi et al., 2016; Zhang et al., 2018b) (Figures 1F and S1D–S1G). We then generated mixed cultures of glutamatergic and GABAergic by co-culturing Ngn2 and AD iN cells obtained from these clones and analyzed them by immunofluorescence. We found a punctuated HA staining pattern along dendrites, often co-localizing with the synaptic marker Synapsin-1 (0.74 ± 0.05 Mander's Coeff.) (Figures 1G, 1I, and S1H). Thus, about 70% of NLGN4 puncta localize to synapses. We next wondered whether NLGN4 is preferentially localized to a specific type of synapse. We labeled the cultures with antibodies to Homer-1, PSD-95, or VGluT2 as markers of excitatory synapses or the Vesicular inhibitory amino acid transporter (VGAT) and Gephyrin as markers of inhibitory synapses (Figures 1J, S1I, and S1J). We observed that more than 80% of excitatory synapses were occupied by NLGN4-HA signal whereas less than 40% of inhibitory synapses were NLGN4-HA positive (Figures 1K and S1K). To better define the localization of NLGN4, we performed Stochastic Optical Reconstruction Microscopy (STORM) Imaging with markers for pre- (Synapsin-1) and post- (PSD-95) synaptic compartments. In many synaptic boutons, the NLGN4-HA signal was juxtaposed to the signal of Synapsin-1 and almost perfectly overlapping the signal of PSD-95 suggesting a postsynaptic localization for NLGN4 (Figures 1L and S1L). In summary, we found that the NLGN4 expression pattern differs between mouse and human brain with predominant expression of human NLGN4 in cortex, that human neurons derived from ESCs produce cell type-dependent levels of NLGN4 and that the majority of synaptic human NLGN4 is localized to excitatory synapses.

NLGN4 Overexpression in Human Neurons Modulates Excitatory Synaptic Transmission

Nlgn4-like KO mouse showed a phenotype in inhibitory synapses but overexpression of human NLGN4 in mouse neurons specifically altered excitatory synaptic transmission (Chanda et al., 2016; Zhang et al., 2009). Since overexpression studies were limited so far to mouse cultures, we wanted to assess the effect of NLGN4 overexpression in human neurons. As shown above (Figure 1E), excitatory Ngn2 iN cells are devoid

Figure 1. Human NLGN4 Is Expressed in Cortex and Localizes to Excitatory Postsynaptic Compartments

(A) Amino acid conservation between Nlgns in mouse (Nlgn) and human (NLGN).

(B) Analysis of NLGN4 protein (immunoblot, top) and RNA (qPCR, bottom) in the adult human brain. Bars represent technical replicates.

(C) Expression of NLGN4 in tested areas shown in a representation of the human brain. Dark red represents high, light red low, blue not determined.

(D) Excitatory neurons are generated by Ngn2; inhibitory neurons are generated by Ascl1 and Dlx2 (AD).

(E) NLGN4 protein (top) and RNA (bottom) in Ngn2- and AD-iN cell cultures at day 42.

(F) Schematics of gene targeting strategy used to generate $NLGN4^{HA}$ ESCs line using rAAV vectors. SP: signal peptide.

(G and H) Representative images of NLGN4-HA stain (G) and co-stain (H) with synaptic markers Synapsin-1 and VGluT2. Arrowhead points to a NLGN4/Synapsin1/vGluT2 co-localization.

(I) Quantification of HA signal overlapping Synapsin-1 signal.

(J) Representative images of co-stain of NLGN4-HA with synaptic markers VGluT2, PSD-95, Homer-1, Gephyrin, and VGAT.

(K) Co-localization analysis of NLGN4-HA signal with synaptic markers.

(L) Representative dSTORM images of single synapses co-stained with NLGN4-HA and Synapsin-1 (top) or PDS-95 (bottom). All images are from endogenously tagged $NLGN4^{HA}$ knock-in AD iN cells mixed with WT Ngn2 iN cells cultured with mouse glia for 5 weeks. MAP2 (blue) is used to identify dendrites.

Scale bars: 20 μm (G), 5 μm (H and J), and 100 nm (L). Data are represented as mean ± SEM and n = 3. See also Figure S1.

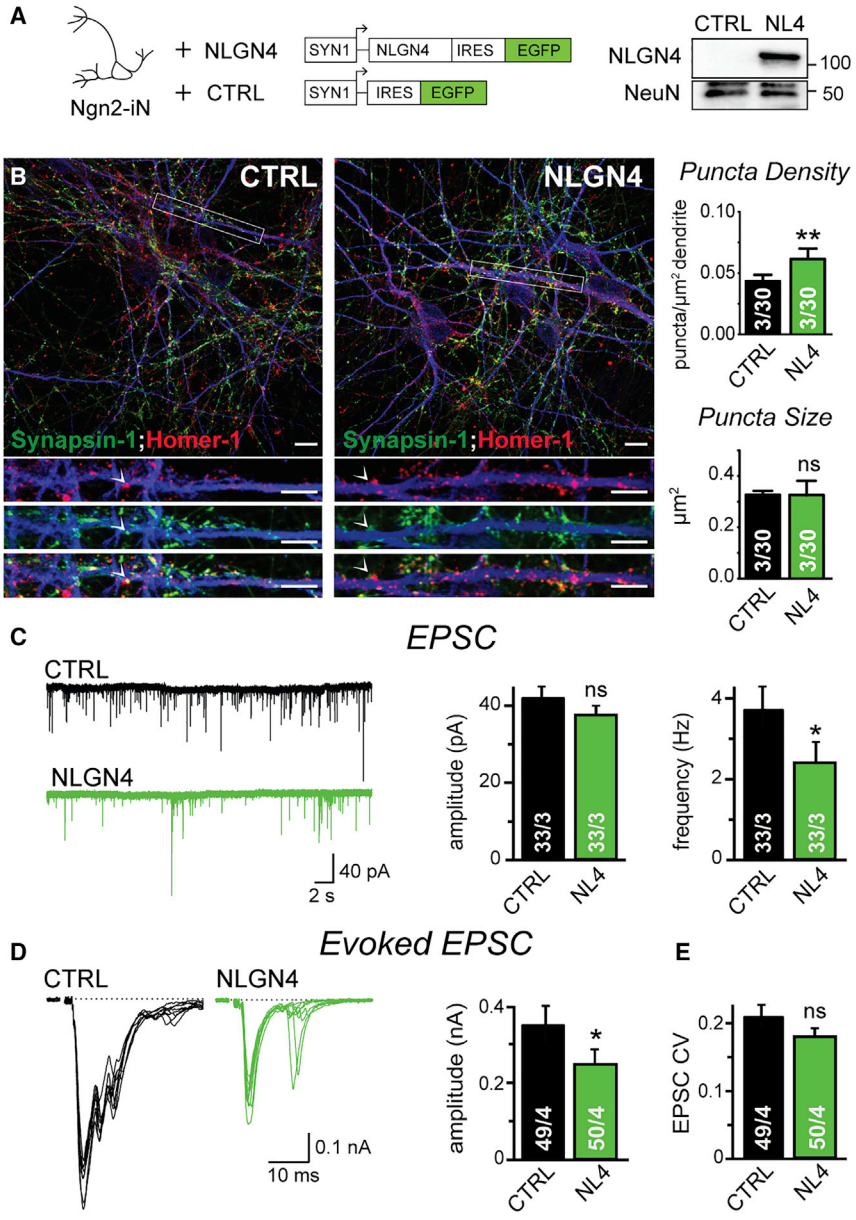

Figure 2. NLGN4 Overexpression in Human Neurons Modulates Excitatory Synaptic Transmission

(A) Schematic of lentiviral vectors used and immunoblot of iN cells transduced with NLGN4 (NL4) or EGFP (CTRL).

(B) Representative images and quantification of puncta density and size in dendrites labeled with Synapsin-1, Homer-1, and MAP2. The arrowhead shows an example of Synapsin1 and Homer1 co-localization.

(C) Example traces (left) and quantification for EPSC amplitudes and frequencies (right).

(D) Example traces and quantification of amplitude for evoked EPSCs.

(E) Quantification of co-efficient of variation (CV) for evoked EPSCs recorded from Ngn2-iN cells with NL4 or CTRL. Analyses are performed at day 35.

Scale bars: 20 μm (upper panel in B) and 5 μm (lower three panels in B). Numbers of neurons/independent cultures analyzed are shown in the bars. Data are represented as mean ± SEM and n = 3. $^{**}p < 0.01$, $^{*}p < 0.05$. See also Figure S2.

of NLGN4 protein and thus serve as an excellent platform to assess the effect of NLGN4 gain of function. We transduced Ngn2 iN cells with lentiviruses expressing both NLGN4 and enhanced green fluorescent protein (EGFP) as a marker to identify transduced cells and confirmed expression by immunoblotting (Figure 2A). Synaptic properties of control and NLGN4-expressing neurons were analyzed 5 weeks later. NLGN4-expressing cells contained more Synapsin-1/Homer-1-positive puncta along their dendrites than control neurons whereas puncta intensity and size were unchanged, suggesting that NLGN4 overexpression increased synapse numbers (Figures 2B and S2A). Remarkably, however, electrophysiological recordings showed that NLGN4 overexpression decreased the frequency (but not amplitude) of spontaneous excitatory postsynaptic currents (sEPSCs), which represent mostly miniature EPSCs in these type of cultures, i.e., non-action potential triggered synaptic transmission (Figure 2C; Zhang et al., 2013). Moreover, NLGN4 overexpression decreased the amplitude of action potential-triggered synaptic transmission (Figure 2D). One possible explanation of these observations is that NLGN4 overexpression induces the formation of new synapses but at the same time decreases the release probability of all synapses, resulting in a net decrease of synaptic transmission. To test this hypothesis, we calculated the coefficient of variation of evoked EPSCs, which mostly reflects the presynaptic release probability, but did not identify any changes (Figure 2E). These experiments suggest that NLGN4 overexpressed induced the formation of new synapses, but simultaneously decreased the fraction of synapses that are functional.

The R704C Mutation Increases Excitatory but Not Inhibitory Synapse Formation by a Postsynaptic Mechanism

To gain insight into the role of NLGN4 and its association with ASD, we generated isogenic ESCs carrying a loss-of-function allele ($NLGN4^{KO}$) (Figures S3A–S3D). Many ASD-associated mutations lead to abolishment of NLGN4 expression, suggesting a loss-of-function pathomechanism (Jamain et al., 2003; Laumonnier et al., 2004; Lawson-Yuen et al., 2008; Talebizadeh et al., 2006). Other mutations, such as the R704C, may rather alter NLGN4 function (Chanda et al., 2016; Etherton et al., 2011;

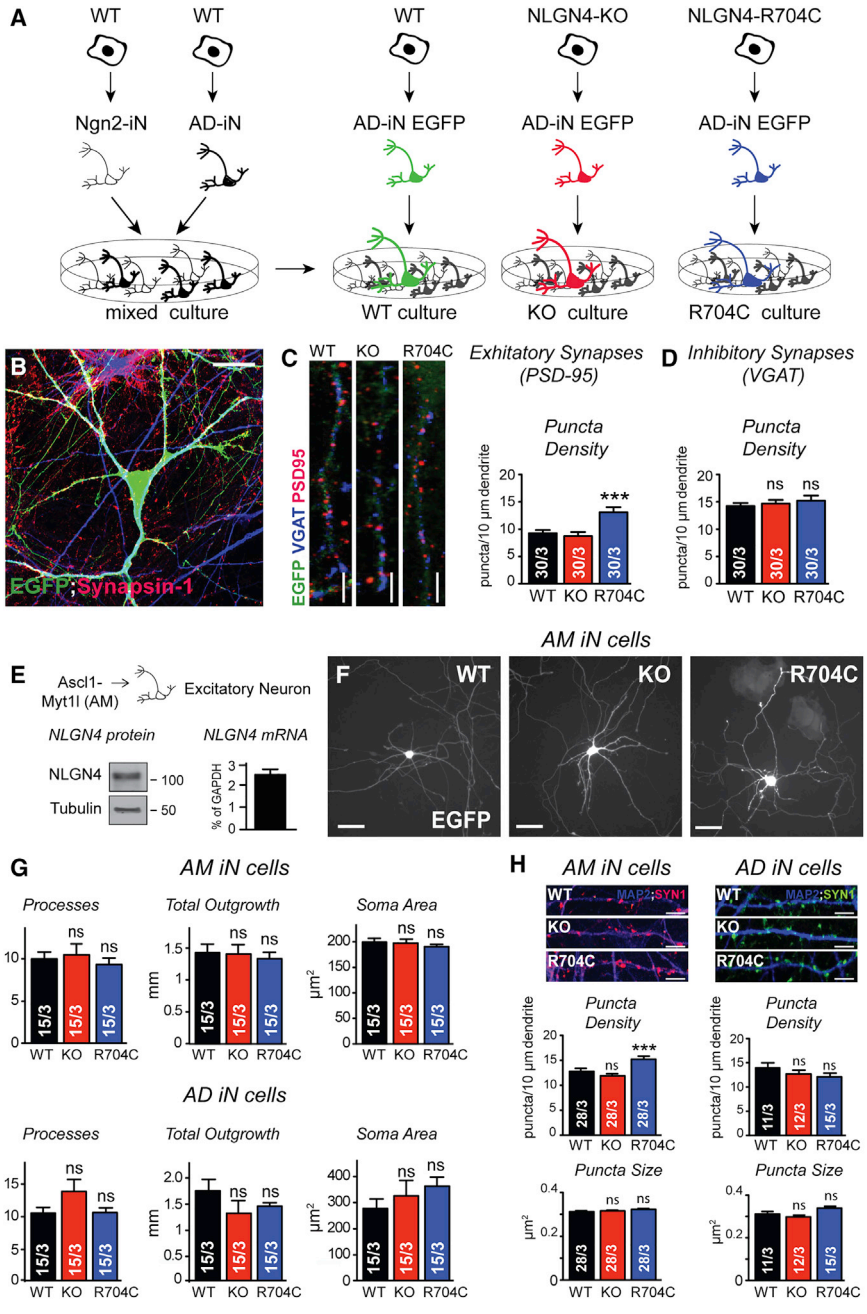

Figure 3. The R704C Mutation Increases Excitatory Synapse Formation

(A) EGFP labeled WT, KO, and R704C AD-iN cells sparsely spiked into standardized cultures consisting of mixed Ngn2 and AD-iN cells to minimize variability.

(B) Representative image of the cultures (labeled with EGFP and Synapsin-1).

(C and D) Representative images and quantification of puncta density for excitatory (PSD-95) (C) and inhibitory synapses (VGAT) (D) at day 42. Dendrites were labeled with MAP2 (blue).

(E) Excitatory neurons expressing NLGN4 protein induced from ESCs by Ascl1 and Myt1l (AM). NLGN4 protein (immunoblot, left) and RNA (qPCR, right) levels in AM-iN cells at day 42.

(F and G) Representative images (F) and quantification (G) of morphology of excitatory AM-iN and inhibitory AD-iN cells differentiated from WT, KO, and R704C sparsely transfected with EGFP for visualization of cellular processes belonging to a single cell in high-density cultures.

(H) Representative images and quantification of puncta density and size for Synapsin-1 in dendrites immunolabeled with MAP2 from WT, KO, and R704C in AM-iN and AD-iN cells.

Scale bars: 20 µm for (B), 50 µm for (F), and 5 µm for (C) and (H). Numbers of total neurons/independent cultures analyzed are shown in the bars. Data are represented as mean ± SEM and n = 3. ***p < 0.001. See also Figure S3.

Yan et al., 2005). To study the effect of the R704C mutation in the context of human neurons, we generated ESCs containing a NLGN4 R704C knock-in allele (NLGN4^{R704C}) (Figures S3E–S3G). For subsequent analyses, we used two clones per line and employed the parental ESC line at similar passage number as a wild-type (WT) control. Immunoblotting confirmed the absence of NLGN4 protein in NLGN4^{KO} AD iN cells, further validating the specificity of the NLGN4 antibody. NLGN4^{R704C} neurons, conversely, showed expression levels comparable to WT (Figure S3H). To characterize the NLGN4 mutant neurons, we first assessed the morphology of synapses. To reduce variability, we generated unlabeled WT neurons composed of both excitatory Ngn2 iN cells and inhibitory AD iN cells, providing homogeneous neuronal cultures. We then differentiated WT, NLGN4^{KO}, and NLGN4^{R704C} mutant ESCs into neurons using the AD protocol which produces neurons that show robust NLGN4 protein expression (Figure 1E), labeled the cells with EGFP, and spiked-in neurons of the three different genotypes into the mixed cultures (Figures 3A and 3B). We then used confocal microscopy to image PSD-95 puncta associated with EGFP-positive dendtrites as marker for excitatory synapses. We found that NLGN4^{R704C} neurons exhibited a significant increase of the puncta density (Figures 3C and S3I). Notably, none of the mutations affected inhibitory synapses (Figures 3D and S3J). To further support these findings, we quantified again the excitatory synapses co-labeling with both Synapsin-1 and PSD-95 (Figure S3K). Since the presynaptic input is almost exclusively provided by WT cells in these cultures, the mutation must affect the number of excitatory synapses by a postsynaptic action. This observation is consistent with our imaging data (Figure 1L) and with the notion that neuroligins are adhesion proteins of the postsynaptic membrane (Graf et al., 2004; Song et al., 1999). To assess the effect of the R704C

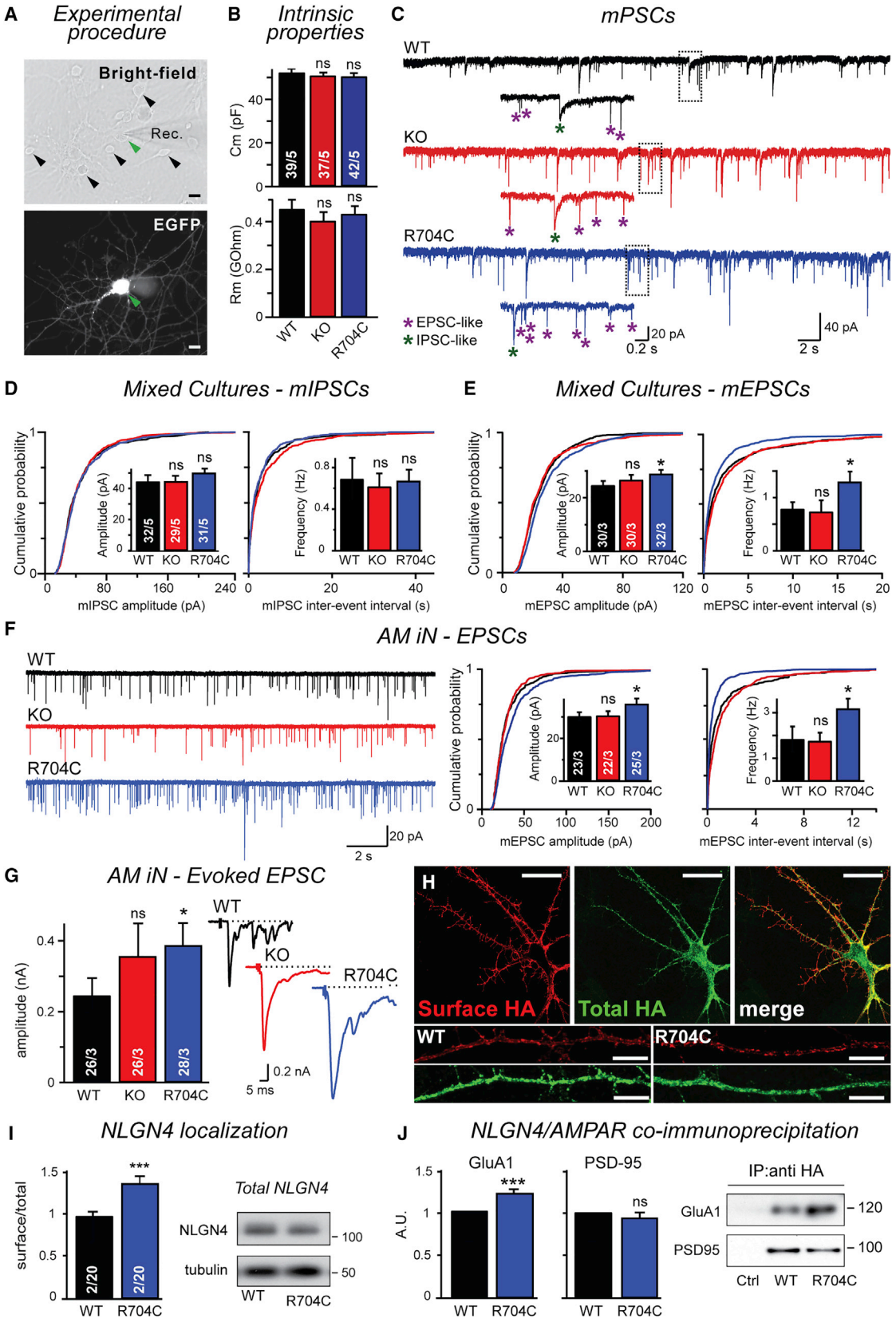

(legend on next page)

mutation in both excitatory and inhibitory neurons, we performed morphological analysis of NLGN4 mutant cells differentiated either into pure excitatory or pure inhibitory neurons. Since Ngn2-iN cells do not express NLGN4 protein (Figure 1E), we used an alternative protocol to generate excitatory neurons from ESCs using Ascl1 and Myt1l (AM) (Chanda et al., 2014; Yang et al., 2017), which we found to express NLGN4 protein at 4 weeks of differentiation (Figures 3E and S3L). Morphometric analysis revealed no changes in cell morphology of either NLGN4^{KO} or NLGN4^{R704} cells (Figures 3F, 3G, and S3M–S3O). Next, we assessed the formation of synapses in the separate excitatory and inhibitory cultures. The observed increase of synapses on NLGN4^{R704} mutant dendrites was well replicated in excitatory AM iN cells but not in the inhibitory AD iN cells (Figures 3H and S3P). These results demonstrate that NLGN4 specifically affects the formation of excitatory synapses in both excitatory and inhibitory neurons. Moreover, NLGN4^{R704C} does not represent a loss-of-function mutation.

Increased Strength of Excitatory Synapses of NLGN4^{R704C} Human Neurons

Finally, we sought to characterize NLGN4 mutant neurons electrophysiologically with an emphasis on functional neurotransmission. Again, we employed the sparse spike-in co-culture system with fluorescently labeled cells of WT, NLGN4^{KO}, or NLGN4^{R704C} genotypes (Figure 3A). EGFP-positive cells were identified by live fluorescence microscopy and specifically recorded using a patch-clamp pipette (Figure 4A). Passive membrane properties were unchanged in either mutant condition (Figure 4B), corroborating our previous findings that mutant cells do not exhibit morphological changes (Figure 3G). To assess synaptic properties, we first isolated miniature excitatory postsynaptic currents (mEPSCs) and miniature inhibitory postsynaptic currents (mIPSCs) from the recordings based on the rapid or slow recovery kinetics (Figures 4C and S4A). Isolated events were then analyzed for number (frequency) and quantal size (amplitude) of synaptic events. mIPSCs frequency and amplitude were similar between NLGN4^{KO}, NLGN4^{R704C}, and control cells (Figure 4D). In contrast, the mEPSCs frequency was significantly increased in the NLGN4^{R704C} neurons (Figure 4E). This finding can be explained by the morphological observation of increased number of excitatory synapses (Figures 3C and 3H). The increase in mEPSC frequency suggests that the observed increased number of excitatory synapses in NLGN4^{R704C} neurons are participating in functional neurotransmission.

Remarkably, we also observed a statistically significant increase of mEPSC amplitudes in R704C mutant cells (Figure 4E). NLGN4^{KO} cells showed a consistent among replicates, but overall not statistically significant trend of increased EPSC amplitudes. Given the specific effects on excitatory synaptic transmission, we sought to corroborate our findings using purely excitatory neurons that also express NLGN4 protein. We therefore characterized NLGN4^{WT}, NLGN4^{KO}, and NLGN4^{R704C} AM iN cells electrophysiologically without co-culture of WT neurons. These recordings exactly reproduced the findings in mixed cultures: both the mEPSCs amplitude and frequency of R704C neurons were significantly increased, while the KO neurons showed no significant changes (Figures 4F and S4B). Measurements of evoked, action potential-triggered synaptic currents confirmed an increase in AMPA receptor-mediated excitatory synaptic transmission in R704C mutant neurons and again a consistent but not significant trend in NLGN4 KO neurons (Figure 4G). The synaptic phenotypes were specific for excitatory neurotransmission as they were not observed in inhibitory synapses (Figure S4C). Unlike the increased mEPSCs frequency, the effect on mEPSCs amplitude in NLGN4^{R704} neurons cannot be explained by the increased number of synapses detected morphologically. Instead, the effect may be caused by a role of the NLGN4 cytoplasmic domain in regulating synaptic AMPA-type glutamate receptors recruitment or stability. To test this hypothesis, we first asked whether the R704C mutation impairs the surface exposure of NLGN4. To specifically label the surface NLGN4, we performed live labeling of Ngn2 iN cells transfected with WT or R704C mutant NLGN4-HA. We then fixed the stained cells to detect total NLGN4 using an anti-HA antibody from a different species (Figure 4H). The total levels of NLGN4 expression were not affected by the R704C mutation as determined by immunoblotting (Figure 4I, right) but the surface localization of NLGN4^{R704C} increased relative to total levels compared to WT NLGN4 (Figures 4I and S4D). In mouse neurons, the R704C mutation is known to affect affinity of Nlg3 for AMPA receptors (Chanda et al., 2016). To test whether NLGN4 interacts with AMPAR in the context of human neurons, we set up a co-immunoprecipitation experiment in Ngn2 iN cells. Ngn2 iN cells were infected with either HA-NLGN4, HA-NLGN4^{R704C}, or EGFP (Figure S4E). Upon immunoprecipitation with anti-HA

Figure 4. Increased Strength of Excitatory Synapses of NLGN4^{R704C} Human Neurons

(A) Representative images of patch clamping of EGFP-labeled AD-iN cells in mixed cultures.

(B) Quantification of intrinsic properties of spiked-in AD-iN cells in mixed cultures differentiated from wild-type H1 (WT), NLGN4^{KO} (KO), and NLGN4^{R704C} (R704C) cells.

(C–E) Example mPSCs traces recorded in the presence of TTX (C), quantification of mIPSCs amplitudes and frequencies (D), and quantification of mEPSCs amplitudes and frequencies from spiked-in AD-iN cells WT, KO, and R704C at day 42 (E).

(F and G) Example traces and quantification of sEPSCs (F) and evoked EPSC amplitudes recorded from AM-iN cells WT, KO, and R704C cells at day 42 (G).

(H) Representative images of surface (live staining) and total HA signal (fixed staining) in day 28 Ngn2 iN cells expressing NGLN4-HA or NLGN4^{R704C}-HA.

(I) Quantification of surface localized NLGN4 relative to total NLGN4 in Ngn2 iN cells (left) expressing NGLN4-HA (WT) or NLGN4^{R704C}-HA (R704C). Right panel, immunoblotting from the same cultures shows comparable levels of total NLGN4 protein in WT and R704C.

(J) NLGN4 co-immunoprecipitates with GluA1 and PSD-95. The R704C mutation enhances co-immunoprecipitation of NLGN4 with GluA1. Protein lysates from Ngn2 iN cells expressing NLGN4 WT, R704C, or EGFP (Ctrl) immunoprecipitated with HA antibodies and blotted for the AMPAR-GluA1 and for PSD-95. Left, quantification of the relative levels of GluA1 and PSD95 in the immunoprecipitates.

Scale bars: 50 μm for (A) and (H), top, and 10 μm (H), bottom. Data are represented as mean ± SEM and n = 3. Numbers of neurons/independent cultures analyzed are shown in the bars. *p < 0.05, ***p < 0.001. See also Figure S4.

antibodies, we detected GluA1 and PSD-95 specifically in the NLGN4-infected cells but not in control cells (Figure 4J). While the levels of PSD-95 enrichment was similar between WT and R704C, we found a marked increase of GluA1 protein in the R704C pull downs compared to WT (Figure 4J). These experiments suggest that NLGN4 is physically associated with AMPARs in human neurons and that the R704C mutation enhances this association.

DISCUSSION

To assess the function of NLGN4, we took advantage of the recent advances in stem cell biology providing human neuronal cell models that approach functional maturation levels of primary rodent cultures (Espuny-Camacho et al., 2013; Maroof et al., 2013; Shi et al., 2012; Zhang et al., 2013). Human cells eliminate the problem of poor gene conservation and possible altered gene function in animal model organisms. We found important differences between the human *NLGN4* and its closest mouse ortholog. First, while mouse *Nlgn4* is primarily expressed in brain stem, retina, and spinal cord (Hoon et al., 2011), we found most robust NLGN4 protein expression in human cortex and parts of the striatum, structures regulating higher cognitive functions, such as language, social interaction, and emotions, which are affected in ASD (Amaral et al., 2008). Second, elegant studies demonstrated that mouse *Nlgn4* is localized to glycinergic synapses (Hoon et al., 2011; Zhang et al., 2018a). In contrast, in human neurons NLGN4 protein preferentially localized to excitatory synapses and only a subset of inhibitory synapses. Third, the *Nlgn4* KO mice revealed a functional role of Nlgn4 for inhibitory synaptic transmission in mice (Hammer et al., 2015; Hoon et al., 2011; Zhang et al., 2018a). These studies were at odds with NLGN4 overexpression studies, which showed effects exclusively on excitatory neurotransmission, and paradoxically caused an increase in excitatory synapse numbers but a decrease in overall excitatory synaptic strength (Bemben et al., 2015; Chanda et al., 2016; Zhang et al., 2009). We observed the same overexpression phenotypes described in mouse, suggesting that the species context is not responsible for the puzzling findings. More importantly, manipulation of endogenous *NLGN4* in human neurons unambiguously demonstrated that NLGN4 operates in excitatory synapses. We found that the NLGN4 KO and the R704C mutations produced different phenotypes in excitatory synaptic transmission. NLGN4 KO cells displayed a trend toward increased synaptic strength, while R704C cells exhibited a highly significant enhancement of synaptic strength that manifested in an increase in the amplitude and frequency of AMPAR-mediated mEPSCs and in the amplitude of AMPAR-mediated evoked EPSCs. In addition, the R704C mutation caused a significant increase in excitatory synapse numbers. Thus, the R704C mutation in human caused a gain-of-function effect. Strikingly, the effect of the R704C mutation is opposite to the effect of Nlgn3-R704C mouse knock-in mutation which selectively decreased AMPAR-mediated synaptic responses instead of increasing them (Etherton et al., 2011; Chanda et al., 2016). The R704C sequence context is highly conserved in all neuroligins; the fact that the same knock-in mutation in different neuroligins specifically alters AMPAR-mediated responses suggests similar functions of this sequence, but the observation that the effect of the R704C mutation on AMPA responses is opposite between Nlgn3 and NLGN4 indicates that the overall neuroligin isoform dictates the specific function of the shared sequence context. It should be noted that our studies do not suggest a common molecular path for ASD pathogenesis—quite the contrary. A range of different neuroligin mutations in neuroligin isoforms have now been associated with ASD; it is increasingly clear that these neuroligins perform distinct functions (Zhang et al., 2015; Chanda et al., 2016), and our current data show in conjunction with earlier studies that different mutations in the same neuroligin can produce different functional effects. Thus, it seems more likely that any functional change in a neuroligin can predispose to ASD instead of a common functional change that produces a particular downstream consequence. What is the molecular function of NLGN4 in excitatory synapses? The observation that NGLN4 overexpression leads to a decrease in synaptic events but an increase in the number of synapses is in line with previous observations in mouse and could be explained if NLGN4 interferes with excitatory postsynaptic function yet induces formation of non-functional synapses. The observation that R704C increases excitatory synaptic transmission suggests that the mutation changes the availability of functional AMPA receptors at the postsynaptic compartment. We observed that the R704C not only changes the subcellular localization of NLGN4 but may increase also the affinity of NLGN4 to AMPARs. This observation is consistent with previous findings in the R704C-Nlgn3 mouse (Etherton et al., 2011) and it provides a possible mechanistic explanation for the increase in EPSC amplitude observed in iN cells. Our observation that NLGN4 is also expressed extrasynaptically supports the notion of NLGN4 controlling the localization of critical postsynaptic proteins like AMPA receptors. In summary, it is tempting to speculate that the intracellular NLGN4 domain acts as "negative control" for synaptogenesis promoted by other neuroligins present in excitatory synapses and in a parallel way controls postsynaptic function by selective AMPA receptor trafficking in and outside the synapse. The elucidation of such mechanisms and additional molecular mediators of postsynaptic neuroligin regulation will be critical in the future to identify candidate targets for a potential therapeutic intervention of ASD caused by neuroligin mutations.

STAR★METHODS

Detailed methods are provided in the online version of this paper and include the following:

- KEY RESOURCES TABLE
- LEAD CONTACT AND MATERIALS AVAILABILITY
- EXPERIMENTAL MODEL AND SUBJECT DETAILS
  - Samples from human subjects
  - Mouse husbandry
  - Cell lines details
  - Primary cultures details
- METHODS DETAILS
  - Cell Culture
  - Lentiviral generation
  - Generation of iN cells
  - Conservation analysis

- Immunofluorescence experiments
- Immunoprecipitation experiments
- RNA-sequencing experiments
- Gene Expression Analyses
- Analysis of dendritic arborizations
- Synaptic puncta density analysis
- Colocalization analysis
- AAV production
- Gene Targeting
- Electrophysiology
- Rapid Autopsy
- Stochastic Optical Reconstruction Microscopy (STORM) Imaging:

- QUANTIFICATION AND STATISTICAL ANALYSIS
- DATA AND CODE AVAILABILITY

SUPPLEMENTAL INFORMATION

Supplemental Information can be found online at https://doi.org/10.1016/j.neuron.2019.05.043.

ACKNOWLEDGMENTS

We thank members of the Wernig and Südhof labs for comments and help during the study and Rahul Sinha for advising on RNA-seq experiments. We also thank the Stanford Neuroscience Microscopy Service, supported by NIH NS069375 and Donor Network West - San Ramon, CA, for providing human brain samples. The work was supported by NIH grant R01MH092931 (to M.W. and T.C.S.) and the New York Stem Cell Foundation-Robertson Stem Cell Award (M.W.). M.W. is a Tashia and John Morgridge Faculty Scholar, Child Health Research Institute at Stanford, and a Howard Hughes Medical Institute Faculty Scholar. T.C.S. is a Howard Hughes Medical Institute Investigator.

AUTHOR CONTRIBUTIONS

All authors planned the experiments, S.G.M., S.C., N.Y., J.A.J., G.V., J.T., B.Z., S.M., I.Y., and H.S. performed the experiments, S.G.M., S.C., N.Y., T.C.S., and M.W. analyzed the data, and S.G.M., S.C., T.C.S., and M.W. wrote the paper.

DECLARATION OF INTERESTS

The authors declare no competing interests.

Received: August 28, 2018
Revised: April 17, 2019
Accepted: May 28, 2019
Published: June 27, 2019

REFERENCES

Amaral, D.G., Schumann, C.M., and Nordahl, C.W. (2008). Neuroanatomy of autism. Trends Neurosci. *31*, 137–145.

Beaudet, A.L. (2007). Autism: highly heritable but not inherited. Nat. Med. *13*, 534–536.

Bemben, M.A., Nguyen, Q.-A., Wang, T., Li, Y., Nicoll, R.A., and Roche, K.W. (2015). Autism-associated mutation inhibits protein kinase C-mediated neuroligin-4X enhancement of excitatory synapses. Proc. Natl. Acad. Sci. USA *112*, 2551–2556.

Bolliger, M.F., Pei, J., Maxeiner, S., Boucard, A.A., Grishin, N.V., and Südhof, T.C. (2008). Unusually rapid evolution of Neuroligin-4 in mice. Proc. Natl. Acad. Sci. USA *105*, 6421–6426.

Chanda, S., Marro, S., Wernig, M., and Südhof, T.C. (2013). Neurons generated by direct conversion of fibroblasts reproduce synaptic phenotype caused by autism-associated neuroligin-3 mutation. Proc. Natl. Acad. Sci. USA *110*, 16622–16627.

Chanda, S., Ang, C.E., Davila, J., Pak, C., Mall, M., Lee, Q.Y., Ahlenius, H., Jung, S.W., Südhof, T.C., and Wernig, M. (2014). Generation of induced neuronal cells by the single reprogramming factor ASCL1. Stem Cell Reports *3*, 282–296.

Chanda, S., Aoto, J., Lee, S.-J., Wernig, M., and Südhof, T.C. (2016). Pathogenic mechanism of an autism-associated neuroligin mutation involves altered AMPA-receptor trafficking. Mol. Psychiatry *21*, 169–177.

Chocholska, S., Rossier, E., Barbi, G., and Kehrer-Sawatzki, H. (2006). Molecular cytogenetic analysis of a familial interstitial deletion Xp22.2-22.3 with a highly variable phenotype in female carriers. Am. J. Med. Genet. A. *140*, 604–610.

Delattre, V., La Mendola, D., Meystre, J., Markram, H., and Markram, K. (2013). Nlgn4 knockout induces network hypo-excitability in juvenile mouse somatosensory cortex in vitro. Sci. Rep. *3*, 2897.

Dobin, A., Davis, C.A., Schlesinger, F., Drenkow, J., Zaleski, C., Jha, S., Batut, P., Chaisson, M., and Gingeras, T.R. (2013). STAR: ultrafast universal RNA-seq aligner. Bioinformatics *29*, 15–21.

Espuny-Camacho, I., Michelsen, K.A., Gall, D., Linaro, D., Hasche, A., Bonnefont, J., Bali, C., Orduz, D., Bilheu, A., Herpoel, A., et al. (2013). Pyramidal neurons derived from human pluripotent stem cells integrate efficiently into mouse brain circuits in vivo. Neuron *77*, 440–456.

Etherton, M.R., Tabuchi, K., Sharma, M., Ko, J., and Südhof, T.C. (2011). An autism-associated point mutation in the neuroligin cytoplasmic tail selectively impairs AMPA receptor-mediated synaptic transmission in hippocampus. EMBO J. *30*, 2908–2919.

Franke, B., Figiel, M., and Engele, J. (1998). CNS glia are targets for GDNF and neurturin. Histochem. Cell Biol. *110*, 595–601.

Gilbert, M., Smith, J., Roskams, A.J., and Auld, V.J. (2001). Neuroligin 3 is a vertebrate gliotactin expressed in the olfactory ensheathing glia, a growth-promoting class of macroglia. Glia *34*, 151–164.

Graf, E.R., Zhang, X., Jin, S.-X., Linhoff, M.W., and Craig, A.M. (2004). Neurexins induce differentiation of GABA and glutamate postsynaptic specializations via neuroligins. Cell *119*, 1013–1026.

Hammer, M., Krueger-Burg, D., Tuffy, L.P., Cooper, B.H., Taschenberger, H., Goswami, S.P., Ehrenreich, H., Jonas, P., Varoqueaux, F., Rhee, J.-S., and Brose, N. (2015). Perturbed Hippocampal Synaptic Inhibition and γ-Oscillations in a Neuroligin-4 Knockout Mouse Model of Autism. Cell Rep. *13*, 516–523.

Hoon, M., Soykan, T., Falkenburger, B., Hammer, M., Patrizi, A., Schmidt, K.-F., Sassoè-Pognetto, M., Löwel, S., Moser, T., Taschenberger, H., et al. (2011). Neuroligin-4 is localized to glycinergic postsynapses and regulates inhibition in the retina. Proc. Natl. Acad. Sci. USA *108*, 3053–3058.

Iossifov, I., O'Roak, B.J., Sanders, S.J., Ronemus, M., Krumm, N., Levy, D., Stessman, H.A., Witherspoon, K.T., Vives, L., Patterson, K.E., et al. (2014). The contribution of de novo coding mutations to autism spectrum disorder. Nature *515*, 216–221.

Jamain, S., Quach, H., Betancur, C., Råstam, M., Colineaux, C., Gillberg, I.C., Soderstrom, H., Giros, B., Leboyer, M., Gillberg, C., and Bourgeron, T.; Paris Autism Research International Sibpair Study (2003). Mutations of the X-linked genes encoding neuroligins NLGN3 and NLGN4 are associated with autism. Nat. Genet. *34*, 27–29.

Ju, A., Hammerschmidt, K., Tantra, M., Krueger, D., Brose, N., and Ehrenreich, H. (2014). Juvenile manifestation of ultrasound communication deficits in the neuroligin-4 null mutant mouse model of autism. Behav. Brain Res. *270*, 159–164.

Juette, M.F., Gould, T.J., Lessard, M.D., Mlodzianoski, M.J., Nagpure, B.S., Bennett, B.T., Hess, S.T., and Bewersdorf, J. (2008). Three-dimensional sub-100 nm resolution fluorescence microscopy of thick samples. Nat. Methods *5*, 527–529.

Khan, I.F., Hirata, R.K., and Russell, D.W. (2011). AAV-mediated gene targeting methods for human cells. Nat. Protoc. *6*, 482–501.

Laumonnier, F., Bonnet-Brilhault, F., Gomot, M., Blanc, R., David, A., Moizard, M.-P., Raynaud, M., Ronce, N., Lemonnier, E., Calvas, P., et al. (2004). X-linked mental retardation and autism are associated with a mutation in the NLGN4 gene, a member of the neuroligin family. Am. J. Hum. Genet. *74*, 552–557.

Lawson-Yuen, A., Saldivar, J.-S., Sommer, S., and Picker, J. (2008). Familial deletion within NLGN4 associated with autism and Tourette syndrome. Eur. J. Hum. Genet. *16*, 614–618.

Li, H., Handsaker, B., Wysoker, A., Fennell, T., Ruan, J., Homer, N., Marth, G., Abecasis, G., and Durbin, R.; 1000 Genome Project Data Processing Subgroup (2009). The Sequence Alignment/Map format and SAMtools. Bioinformatics *25*, 2078–2079.

Lisowski, L., Dane, A.P., Chu, K., Zhang, Y., Cunningham, S.C., Wilson, E.M., Nygaard, S., Grompe, M., Alexander, I.E., and Kay, M.A. (2014). Selection and evaluation of clinically relevant AAV variants in a xenograft liver model. Nature *506*, 382–386.

Longo, P.A., Kavran, J.M., Kim, M.-S., and Leahy, D.J. (2013). Transient mammalian cell transfection with polyethylenimine (PEI). Methods Enzymol. *529*, 227–240.

Macarov, M., Zeigler, M., Newman, J.P., Strich, D., Sury, V., Tennenbaum, A., and Meiner, V. (2007). Deletions of VCX-A and NLGN4: a variable phenotype including normal intellect. J. Intellect. Disabil. Res. *51*, 329–333.

Maroof, A.M., Keros, S., Tyson, J.A., Ying, S.-W., Ganat, Y.M., Merkle, F.T., Liu, B., Goulburn, A., Stanley, E.G., Elefanty, A.G., et al. (2013). Directed differentiation and functional maturation of cortical interneurons from human embryonic stem cells. Cell Stem Cell *12*, 559–572.

Marro, S., and Yang, N. (2014). Transdifferentiation of mouse fibroblasts and hepatocytes to functional neurons. Methods Mol. Biol. *1150*, 237–246.

Marshall, C.R., Noor, A., Vincent, J.B., Lionel, A.C., Feuk, L., Skaug, J., Shago, M., Moessner, R., Pinto, D., Ren, Y., et al. (2008). Structural variation of chromosomes in autism spectrum disorder. Am. J. Hum. Genet. *82*, 477–488.

Mlodzianoski, M.J., Juette, M.F., Beane, G.L., and Bewersdorf, J. (2009). Experimental characterization of 3D localization techniques for particle-tracking and super-resolution microscopy. Opt. Express *17*, 8264–8277.

Neale, B.M., Kou, Y., Liu, L., Ma'ayan, A., Samocha, K.E., Sabo, A., Lin, C.-F., Stevens, C., Wang, L.-S., Makarov, V., et al. (2012). Patterns and rates of exonic de novo mutations in autism spectrum disorders. Nature *485*, 242–245.

Notredame, C., Higgins, D.G., and Heringa, J. (2000). T-Coffee: A novel method for fast and accurate multiple sequence alignment. J. Mol. Biol. *302*, 205–217.

O'Roak, B.J., Vives, L., Girirajan, S., Karakoc, E., Krumm, N., Coe, B.P., Levy, R., Ko, A., Lee, C., Smith, J.D., et al. (2012). Sporadic autism exomes reveal a highly interconnected protein network of de novo mutations. Nature *485*, 246–250.

Pak, C., Danko, T., Zhang, Y., Aoto, J., Anderson, G., Maxeiner, S., Yi, F., Wernig, M., and Südhof, T.C. (2015). Human Neuropsychiatric Disease Modeling using Conditional Deletion Reveals Synaptic Transmission Defects Caused by Heterozygous Mutations in NRXN1. Cell Stem Cell *17*, 316–328.

Pampanos, A., Volaki, K., Kanavakis, E., Papandreou, O., Youroukos, S., Thomaidis, L., Karkelis, S., Tzetis, M., and Kitsiou-Tzeli, S. (2009). A substitution involving the NLGN4 gene associated with autistic behavior in the Greek population. Genet. Test. Mol. Biomarkers *13*, 611–615.

Pang, Z.P., Yang, N., Vierbuchen, T., Ostermeier, A., Fuentes, D.R., Yang, T.Q., Citri, A., Sebastiano, V., Marro, S., Südhof, T.C., and Wernig, M. (2011). Induction of human neuronal cells by defined transcription factors. Nature *476*, 220–223.

Papadopoulos, J.S., and Agarwala, R. (2007). COBALT: constraint-based alignment tool for multiple protein sequences. Bioinformatics *23*, 1073–1079.

Patzke, C., Han, Y., Covy, J., Yi, F., Maxeiner, S., Wernig, M., and Südhof, T.C. (2015). Analysis of conditional heterozygous STXBP1 mutations in human neurons. J. Clin. Invest. *125*, 3560–3571.

Russell, D.W., and Hirata, R.K. (1998). Human gene targeting by viral vectors. Nat. Genet. *18*, 325–330.

Sanders, S.J., Murtha, M.T., Gupta, A.R., Murdoch, J.D., Raubeson, M.J., Willsey, A.J., Ercan-Sencicek, A.G., DiLullo, N.M., Parikshak, N.N., Stein, J.L., et al. (2012). De novo mutations revealed by whole-exome sequencing are strongly associated with autism. Nature *485*, 237–241.

Shi, Y., Kirwan, P., Smith, J., Robinson, H.P.C., and Livesey, F.J. (2012). Human cerebral cortex development from pluripotent stem cells to functional excitatory synapses. Nat. Neurosci. *15*, 477–486, S1.

Song, J.Y., Ichtchenko, K., Südhof, T.C., and Brose, N. (1999). Neuroligin 1 is a postsynaptic cell-adhesion molecule of excitatory synapses. Proc. Natl. Acad. Sci. USA *96*, 1100–1105.

Südhof, T.C. (2008). Neuroligins and neurexins link synaptic function to cognitive disease. Nature *455*, 903–911.

Südhof, T.C. (2017). Synaptic Neurexin Complexes: A Molecular Code for the Logic of Neural Circuits. Cell *171*, 745–769.

Talebizadeh, Z., Lam, D.Y., Theodoro, M.F., Bittel, D.C., Lushington, G.H., and Butler, M.G. (2006). Novel splice isoforms for NLGN3 and NLGN4 with possible implications in autism. J. Med. Genet. *43*, e21.

Unichenko, P., Yang, J.-W., Kirischuk, S., Kolbaev, S., Kilb, W., Hammer, M., Krueger-Burg, D., Brose, N., and Luhmann, H.J. (2018). Autism Related Neuroligin-4 Knockout Impairs Intracortical Processing but not Sensory Inputs in Mouse Barrel Cortex. Cereb. Cortex *28*, 2873–2886.

Varoqueaux, F., Aramuni, G., Rawson, R.L., Mohrmann, R., Missler, M., Gottmann, K., Zhang, W., Südhof, T.C., and Brose, N. (2006). Neuroligins determine synapse maturation and function. Neuron *51*, 741–754.

Yan, J., Oliveira, G., Coutinho, A., Yang, C., Feng, J., Katz, C., Sram, J., Bockholt, A., Jones, I.R., Craddock, N., et al. (2005). Analysis of the neuroligin 3 and 4 genes in autism and other neuropsychiatric patients. Mol. Psychiatry *10*, 329–332.

Yang, N., Chanda, S., Marro, S., Ng, Y.H., Janas, J.A., Haag, D., Ang, C.E., Tang, Y., Flores, Q., Mall, M., et al. (2017). Generation of pure GABAergic neurons by transcription factor programming. Nat. Methods *14*, 621–628.

Yi, F., Danko, T., Botelho, S.C., Patzke, C., Pak, C., Wernig, M., and Südhof, T.C. (2016). Autism-associated SHANK3 haploinsufficiency causes Ih channelopathy in human neurons. Science *352*, aaf2669–aaf2669.

Zhang, C., Milunsky, J.M., Newton, S., Ko, J., Zhao, G., Maher, T.A., Tager-Flusberg, H., Bolliger, M.F., Carter, A.S., Boucard, A.A., et al. (2009). A neuroligin-4 missense mutation associated with autism impairs neuroligin-4 folding and endoplasmic reticulum export. J. Neurosci. *29*, 10843–10854.

Zhang, Y., Pak, C., Han, Y., Ahlenius, H., Zhang, Z., Chanda, S., Marro, S., Patzke, C., Acuna, C., Covy, J., et al. (2013). Rapid single-step induction of functional neurons from human pluripotent stem cells. Neuron *78*, 785–798.

Zhang, Y., Chen, K., Sloan, S.A., Bennett, M.L., Scholze, A.R., O'Keeffe, S., Phatnani, H.P., Guarnieri, P., Caneda, C., Ruderisch, N., et al. (2014). An RNA-sequencing transcriptome and splicing database of glia, neurons, and vascular cells of the cerebral cortex. J. Neurosci. *34*, 11929–11947.

Zhang, B., Chen, L.Y., Liu, X., Maxeiner, S., Lee, S.-J., Gokce, O., and Südhof, T.C. (2015). Neuroligins Sculpt Cerebellar Purkinje-Cell Circuits by Differential Control of Distinct Classes of Synapses. Neuron *87*, 781–796.

Zhang, B., Seigneur, E., Wei, P., Gokce, O., Morgan, J., and Südhof, T.C. (2017). Developmental plasticity shapes synaptic phenotypes of autism-associated neuroligin-3 mutations in the calyx of Held. Mol. Psychiatry *22*, 1483–1491.

Zhang, B., Gokce, O., Hale, W.D., Brose, N., and Südhof, T.C. (2018a). Autism-associated neuroligin-4 mutation selectively impairs glycinergic synaptic transmission in mouse brainstem synapses. J. Exp. Med. *215*, 1543–1553.

Zhang, Z., Marro, S.G., Zhang, Y., Arendt, K.L., Patzke, C., Zhou, B., Fair, T., Yang, N., Südhof, T.C., Wernig, M., and Chen, L. (2018b). The fragile X mutation impairs homeostatic plasticity in human neurons by blocking synaptic retinoic acid signaling. Sci. Transl. Med. *10*, 10.

STAR★METHODS

KEY RESOURCES TABLE

REAGENT or RESOURCE	SOURCE	IDENTIFIER
Antibodies		
NLGN4	Everest Biotech	EB11592; RRID:AB_2801590
Synapsin-1	Synaptic System	106 002; RRID:AB_887804
VGAT	Synaptic System	131 003; RRID:AB_887869
VGAT	Synaptic System	131 005; RRID:AB_1106810
MAP2	Abcam	AB5392; RRID:AB_2138153
PSD-95	ThermoFisher	MA1-046; RRID:AB_2092361
Homer-1	Synaptic System	160 002; RRID:AB_2120990
Homer-1	Synaptic System	160 025; RRID:AB_2744655
GFP	Abcam	ab13970; RRID:AB_300798
HA	Covance	MMS-101P-200; RRID:AB_10064068
HA	Cell Signaling	3724; RRID:AB_1549585
Gephyrin	Synaptic System	147 011; RRID:AB_887717
VGluT2	EMD Millipore	AB2251; RRID:AB_1587626
α-Tubulin	Sigma	T5168; RRID:AB_477579
L1CAM	Sigma	SAB4100003; RRID:AB_10743420
NeuN	Millipore	ABN78; RRID:AB_10807945
HA	Covance	MMS-101P-200; RRID:AB_10064068
PSD-95	home-made in Südhof lab	N/A
GluA1	EMD-Millipore	AB1504; RRID:AB_2113602
HA antibody-coupled beads	Thermo Fisher Scientific	88836; RRID:AB_2749815
Chemicals, Peptides, and Recombinant Proteins		
CNQX	Tocris	Cat. No. 0190
Picrotoxin	Tocris	Cat. No. 1128
TTX	Fisher Scientific	Cat. No. 50-753-2807
mTeSR1 medium	Stem Cell Technologies	85850
Accutase	Innovative Cell Technologies	AT-104
Matrigel hESC-Qualified Matrix	Corning	08-774-552
Thiazovivin	BioVision	1681
Polyethylenimine (PEI)	Polysciences Inc.	23966-2
Deposited Data		
RNA-seq	This paper; GEO	GEO: GSE131428
Raw data	This paper; Mendeley data	https://doi.org/10.17632/g3wwzmrjv5.1
Experimental Models: Cell Lines		
Human embryonic kidney (HEK) 293T/17 cells	ATCC	CRL-11268; RRID: CVCL_0063
Human embryonic stem cells (ESCs) line H1	WiCell Research Institute, Inc.	WA01; RRID: CVCL_9771
Experimental Models: Organisms/Strains		
CD1 mice	Charles River	Cat. No. 22
Oligonucleotides		
NLGN4 primers - RT-PCR - FW sequence atggagaagatccgccaag	This paper	N/A
NLGN4 primers - RT-PCR - RV sequence ggggacccctaagtactgct	This paper	N/A
NLGN4 primers - q-RT-PCR- FW sequence gcaagctacggaaacgtcat	This paper	N/A

(*Continued on next page*)

Continued

REAGENT or RESOURCE	SOURCE	IDENTIFIER
NLGN4 primers - q-RT-PCR- RV sequence gatccaggagcccatagttg	This paper	N/A
GAPDH primers - q-RT-PCR-FW sequence catgagaagtatgacaacagcct	This paper	N/A
GAPDH primers - q-RT-PCR-RV sequence agtccttccacgataccaaagt	This paper	N/A
Recombinant DNA		
FUW-TetO-Ngn2- P2A-puromycin	Addgene	52047
FUW-TetO- Ascl1-T2A-puromycin	Addgene	97329
FUW-TetO-Dlx2-IRES-hygromycin	Addgene	97330
FUW-TetO-Myt1l	Addgene	27152
FUW-rtTA	Addgene	20342
SYN1-NLGN4-IRES-EGFP	Chanda et al., 2016	N/A
SYN1-IRES-EGFP	Chanda et al., 2016	N/A
SYN1-NLGN4-HA	This paper	N/A
SYN1-NLGN4-R704C-HA	This paper	N/A
pAAV	Lisowski et al., 2014	N/A
pAd5	Lisowski et al., 2014	N/A
LK03	Lisowski et al., 2014	N/A
pRSV-rev	Addgene	12253
pMDLg/ pRRE	Addgene	12251
pMD2.G	Addgene	12259
FUW-TetO-EGFP	Addgene	30130
FCW-EGFP	This paper	N/A
Software and Algorithms		
GraphPad Prism 6	https://www.graphpad.com	RRID:SCR_002798
Fiji	http://www.imagej.net/Fiji	RRID:SCR_002285
Vutara SRX software 6.04	https://www.bruker.com	N/A
Adobe Illustrator	https://www.adobe.com	RRID:SCR_010279
alignment package PT-Coffee	Notredame et al., 2000	N/A
alignment package COBALT	Papadopoulos and Agarwala, 2007	N/A
RNaseq aligner STAR	Dobin et al., 2013	N/A
SAMtools	Li et al., 2009	http://samtools.sourceforge.net/
MetaMorph	Molecular Devices	RRID: SCR_002368
pCLAMP 10	Molecular Devices	RRID: SCR_011323

LEAD CONTACT AND MATERIALS AVAILABILITY

Further information and requests for resources and reagents should be directed to and will be fulfilled by the Lead Contact, Marius Wernig (wernig@stanford.edu).

EXPERIMENTAL MODEL AND SUBJECT DETAILS

Samples from human subjects

Human samples were obtained at autopsy as a part of the University of Utah School of Medicine's body donor program and Donor Network West, San Ramon, CA. Donor-1 (Figure 1B) is a healthy 87-year-old female who died of age related-causes. Donor-2 (Figure S1C) is a 65-year-old male who died of cancer with no sign of metastasis to the brain. Both donors had no neurological disease or any sign of pathology in the brain. All samples were collected postmortem upon receipt of formal authorization from the next of kin.

Mouse husbandry

All mouse studies were performed according to protocols approved by the Stanford University Administrative Panel on Laboratory Animal Care. All procedures conformed to NIH Guidelines for the Care and Use of Laboratory Animals and were approved by the Stanford University Administrative Panel on Laboratory Animal Care. All mice were housed in the Stanford animal facility under supervision of the Stanford animal care unit; all mice were healthy and not kept in a sterile facility.

Cell lines details

Male human embryonic stem cells (ESCs) line H1 (WA01 WiCell Research Institute, Inc.) were cultured up to passage 29 and authenticated by GTW banding karyotype method, only cells with normal 46, XY karyotype were used for experiments.

Primary cultures details

Mouse glial cells were isolated from the forebrain of newborn (postnatal day 2) male and female wild-type CD1 mice not involved in previous procedures and drug or test naive.

METHODS DETAILS

Cell Culture

Human H1 ESCs were maintained as feeder-free cells in mTeSR1 medium (Stem Cell Technologies). Mouse glial cells were isolated from the forebrain of newborn wild-type CD1 mice (Franke et al., 1998). Briefly, newborn mouse forebrain homogenates were digested with papain and EDTA for 15 min, cells were dissociated by harsh trituration to avoid growing of neurons and plated onto T75 flasks in DMEM (Invitrogen) supplemented with 10% fetal bovine serum (FBS). Upon reaching confluence, glial cells were trypsinized and replated at lower density for a total of three times to remove potential trace amounts of mouse neurons before the glia cell cultures were used for coculture experiment with iN cells.

Lentiviral generation

Lentiviruses were produced as described (Marro and Yang, 2014; Pang et al., 2011) in HEK293T cells (ATCC) by co-transfection with three helper plasmids (pRSV-REV, pMDLg/pRRE and vesicular stomatitis virus G protein expression vector) using Polyethylenimine (PEI) (Longo et al., 2013). Lentiviral particles were ultra-centrifuged, re-suspended in DMEM, aliquoted and stored at −80°C. Only virus preparations with > 90% infection efficiency as assessed by EGFP expression or puromycin resistance were used for experiments. The following lentivirus constructs were used: (i) lentivirus vector (FUW-TetO-Ngn2- P2A-puromycin) expressing Ngn2-P2A-puromycin cassette; (ii) lentivirus vector (FUW-TetO- Ascl1-T2A-puromycin) expressing Ascl1-T2A-puromycin cassette; (iii) lentivirus vector (FUW-TetO-Dlx2-IRES-hygromycin) expressing Dlx2-IRES-hygromycin cassette; (iv) lentivirus vector (FUW-TetO-Myt1l) expressing Myt1l, (v) lentivirus vector (FUW-rtTA) containing rtTA, (vi) lentivirus vector (FCW-EGFP) expressing EGFP. For NLGN4 overexpression experiments: i) lentivirus vector (SYN1-NLGN4-IRES-EGFP) expressing NLGN4-IRES-EGFP cassette, (ii) lentivirus vector (SYN1-NLGN4-HA) expressing NLGN4-HA cassette, (iii) a lentivirus vector (SYN1-IRES-EGFP) containing the IRES-EGFP coding sequence and (iv) lentivirus vector (SYN1-NLGN4-R704C-HA) expressing NLGN4-R704C-HA cassette,

Generation of iN cells

Ngn2-iN and AD-iN cells were generated as described (Yang et al., 2017; Zhang et al., 2013). To generate AM-iN cells, ESCs were treated with Accutase (Innovative Cell Technologies) and plated as dissociated cells in six-well plates (H1 cells: $\sim 5 \times 10^4$ cells/well) on day 0. Cells were plated on plates coated with Matrigel and mTeSR1 containing 2 μM Thiazovivin (Bio Vision). At the same time of plating, lentivirus prepared as described above (1.5 μl/well of six-well plate) was added. On day 1, the culture medium was replaced with N2/DMEM/F12/NEAA (Invitrogen) containing doxycycline (2 μg/ml, Clontech) to induce gene expression, and the culture was retained in the docycycline containing-medium for ~2 weeks. On day 2 and 3 puromycin was used to selected transduced cells. From day 5 to day 7 AraC (4 μM) was added to the media to selected for not dividing cells. On day 6, mouse glial cells were plated on matrigel-coated coverslips ($\sim 5 \times 10^4$ cells/well of 24-well plate). On day 7, iN cells were dissociated using Accutase and plated on glial cells ($\sim 3 \times 10^5$ cells/well of 24-well plate). Cultures were analyzed 5 weeks after induction of the transgenes. Cocultures of excitatory and inhibitory neurons (Ngn2 iN cells and AD iN) were generated as described (Yang et al., 2017).

Conservation analysis

The phylogenetic tree was generated using the alignment package PT-Coffee (Notredame et al., 2000) and the sequence alignment using COBALT (Papadopoulos and Agarwala, 2007).

Immunofluorescence experiments

For live surface labeling, neurons were incubated at room temperature for 5 min with 1X HEPES bath solution, which contained the following (in mM): 140 NaCl, 5 KCl, 2 CaCl2, 2 MgCl2, 10 glucose, and 10 HEPES, with pH adjusted to 7.4 with NaOH, and osmolarity of 300 mOsm. Cultures were then incubated at RT for 20 min with either purified rabbit anti-HA antibody diluted in 1X HEPES bath

solution. Cultures were then gently washed 3 times with 1X HEPES bath solution, followed by fixation for 20 min at RT with 4% (wt/vol) paraformaldehyde (PFA). Following fixation, cultures were washed 3X with DPBS. Cells were then permeabilized and blocked for 1 h with ADB(+), which contains 0.3% Triton X-100 and 5% normal goat serum diluted in DPBS. Primary antibodies were diluted in ADB(+) and cells were incubated O/N at 4C. Cultures were washed 3X and then incubated with Alexa-conjugated secondary antibodies (1:1000, Invitrogen) in ABD(+) for 1 h. Following 3 washes, coverslips for conventional imaging were inverted onto glass microscope slides with Fluoromount-G mounting media (Southern Biotech). For fixed cells labeling the same protocol was used starting from the fixation step. Antibodies used include: Synapsin-1 (rabbit, 1:1,000, Synaptic System, 106 002), VGAT (Rabbit, 1:1000, Synaptic System, 131 003) VGAT (Guinea Pig, 1:1,000, Synaptic System, 131 005), MAP2 (chicken, 1:20,000, Abcam, AB5392), PSD-95 (Mouse, 1:250, ThermoFisher, MA1-046) Homer-1 (rabbit, 1:500, Synaptic System, 160 002), Homer-1 (Guinea pig, 1:1000, Synaptic System, 160 025) GFP (chicken, 1:1000, Abcam, ab13970), HA (mouse, 1:1000, Covance, MMS-101P-200), HA (rabbit, 1:100, Cell Signaling, 3724), Gephyrin (mouse, 1:500, Synaptic System, SY 147 011), VGluT2 (Guinea Pig, 1:1000, EMD Millipore, AB2251).Immunoblotting experiments. Total proteins were extracted from ES, glia or iN cells using urea lysis buffer (75 mM Tris pH 6.8, 3.8% SDS, 4 M Urea, 20% glycerol). Twenty micrograms of protein extracts were separated on 8% SDS-PAGE and analyzed by immunoblot. Antibodies used include NLGN4 (goat, 1:500, Everest Biotech, EB11592), α-Tubulin (mouse, 1:10,000, Sigma, T5168), L1CAM (mouse, 1:1,000, Sigma, SAB4100003), NeuN (rabbit, 1:500, Millipore, ABN78), HA (mouse, 1:500, Covance, MMS-101P-200), PSD-95 (rabbit, 1:1000, home-made in Südhof lab) and GluA1 (rabbit 1:500, EMD-Millipore, AB1504). Experiments were performed in three different cultures replicates.

Immunoprecipitation experiments

For each immunoprecipitation, two 10 cm dishes of iN cells and mouse glia were lysed in 0.25 ml cell lysis buffer containing: 0.5% Triton X-100, 20 mM Tris pH 7.5, 150 mM NaCl, 15 mM $MgCl_2$, 1 mM DTT and 8% glycerol (all from Sigma) and complete protease inhibitor (Roche) for 20 min at 4 C. Supernatant was clarified by centrifugation (17,000 x g, 2 min, 4C) and incubated with 10 μl HA antibody-coupled beads (Thermo Fisher Scientific 88836) for 16 h at 4°C. After binding, the beads were washed extensively in IP buffer (0.5% Triton X-100, 20 mM Tris pH 7.5, 150 mM NaCl, 15 mM $MgCl_2$) and bound proteins were eluted with SDS–PAGE sample buffer. Experiments were performed in three different cultures replicates.

RNA-sequencing experiments

Mature iN cells cultured with mouse glia (6 weeks after transgene induction) were dissociated with Trypsin and FACS-sorted in Trizol LS (Thermo Fisher Scientific). To distinguish from glial cells iN cells were transduced with a lentiviral vector expressing EGFP under the control of CAG promoter (FCW-EGFP) together with the reprogramming transcription factors. Total RNA was extracted following the supplier's recommended method. Samples were processed and libraries were prepared according to the manufacturer's protocol. Sequencing paired-end reads (150 bp) were generated on NextSeq 500 Illumina platforms. Paired-end reads were aligned to the human reference sequence NCBI Build (hg38) with STAR (Dobin et al., 2013). Properly paired reads to the reference were extracted using the SAMtools (Li et al., 2009) function and considered for subsequent analysis. Expression levels of RefSeq-annotated genes were calculated in units of transcripts per kilobase million (TPM). Genes with low TPM (average log2 TPM across all samples less than 1) were removed. Differential expression analysis was performed using Students' t test function "t-test" and genes with P value < 0.05 and at least two-fold expression change were defined as significant.

Gene Expression Analyses

For RT-PCR analyses of pooled cultured cells or brain samples, RNA was isolated using Trizol (Thermo Fisher Scientific) and reverse transcribed with Superscript III (Invitrogen). mRNA levels were quantified using the following NLGN4 specific primers: 5′-atggaga agatccgccaag-3′ and 5′-ggggacccctaagtactgct-3′ producing a band of 725 bp. For quantitative RT-PCR analyses, the RNA was treated with DNase (Applied Biosystems), and reverse transcribed with Superscript III (Invitrogen). mRNA levels were quantified by real-time PCR assay using the Applied Biosystems 7900HT Fast real-time PCR system and RQ analysis software. Titrations of total human cerebral cortex RNA were included in each experiment, and only primers that demonstrated a linear amplification with R2 values of > 0.98 were included. For NLGN4 the following primers were used: 5′-gcaagctacggaaacgtcat-3′ and 5′-gatcca ggagcccatagttg-3′, for GAPDH: 5′-catgagaagtatgacaacagcct-3′ – 5′-agtccttccacgataccaaagt-3′. Expression values were expressed as percent of GAPDH using the formula: 2^{-CT} NLGN4/2^{-CT} GAPDH × 100. Data shown represent the average of the mean values and SEM from 3 independent technical replicates for the human brain samples and three different cultures replicates (biological replicate) for iN cells.

Analysis of dendritic arborizations

Immunofluorescence was performed on mature iN cells using FCW-EGFP plasmid-sparse transfection with Calcium Phosphate method. Images were acquired using a Zeiss digital camera, attached to a Zeiss inverted microscope with a 20x objective. Images from 20 neurons per condition (per n=1) were reconstructed using the MetaMorph neurite application, scoring for total neurite outgrowth, number of processes, neurite branch points, and cell body area. For all experiments, the experimenter was blind to the genotype condition. Experiments were performed in three different cultures replicates.

Synaptic puncta density analysis

Immunofluorescence was performed on mature iN cells using antibodies against MAP2 (marker for dendrites) and synaptic markers: Homer-1, PSD-95, Synapsin-1, VGAT. Confocal images were acquired with a Zeiss LSM510 laser-scanning confocal microscope using a 63x 1.4 NA oil objective. Z stacked images from 20 random fields per condition (per n=1) were converted to maximal projection images and analyzed using MetaMorph software. Cell bodies were masked and number of puncta was normalized over total MAP2 positive area (puncta density) or average MAP2 intensity (puncta intensity). Puncta size and intensity were also calculated. For all experiments, the experimenter was blind to the genotype condition. Experiments were performed in three different cultures replicates.

Colocalization analysis

The fraction of intensity of one channel that is located in pixels containing above threshold signal in another channel (Mander's Coefficient) was quantified using ImageJ plugin JACoP. Experiments were performed in three different cultures replicates.

AAV production

Targeting rAAV were produced in HEK292T cells by co-transfection of pAAV (25 μg), helper adenovirus type 5 (pAd5) (25 μg), and LK03 (25 μg) (Lisowski et al., 2014) per T225 culture flask using calcium phosphate. Cells were harvested 72 h after transfection in PBS/1 mM EDTA and following three freezing thawing cycle. AAVs were collected from cytoplasm using Benzonase (EMD Chemical Inc, Merck 1.01695.002) at a final concentration of 250 units/ml at 37°C for 1 h. Followed by clearing the suspension from cell debris by centrifugation (2,000 x g for 15 min). Supernatant was used to transduce the cells with a dilution factor of 1:1000.

Gene Targeting

$NLGN4^{HA}$, $NLGN4^{KO}$ and $NLGN4^{R704C}$ ESC lines were obtained by recombinant adeno associated virus (rAAV) – mediated homology recombination. The rAAV targeting vector was designed to carry two homology arms separated by a positive selection cassette. Drug-resistant clones that were generated by correct homologous recombination were identified by PCR with primers external to the homology arms and the selection cassette was removed from these clones by transient expression of FlpE or Cre recombinase. Random integrations of the rAAV targeting vector were ruled out by Southern Blot analysis using a Neomycin probe (not shown).

For $NLGN4^{HA}$ a selection cassette containing a splice acceptor (SA) followed by an internal ribosomal entry site (IRES) and the Neomycin resistance gene (NEO) with a polyadenylation signal (PA) was used. HA sequence was inserted in the exon 3 of the NLGN4 gene after the signal peptide (SP) together with a neomycin resistance cassette (NEO) surrounded by flp-recombination sites (FRT) as a selectable marker for recombination events. ES cells were infected with rAAV and selected for 8 days in media containing G418 Sulfate selective antibiotic (GIBCO). 5 resistant clones were picked for $NLGN4^{HA}$ and 2 independent clones with the targeted $NLGN4^{HA}$ allele were chosen for further analysis. 40 resistant clones were picked for $NLGN4^{KO}$, 10 resistant clones were picked for $NLGN4^{R704C}$. Clones were and tested by PCR, Sanger sequencing and immunoblot as described in the figure legend.

For $NLGN4^{KO}$ a selection cassette containing a phosphoglycerate kinase (PGK) promoter followed the Neomycin resistance gene (NEO) with a polyadenylation signal (PA) was used. Selection cassette was inserted into the first coding exon (exon 3) at a position that is 84 nucleotides downstream of the coding region for the signal peptide, creating a premature stop codon. Neomycin resistant colonies were picked, expanded and screened using two sets of primers external to the homology arms. Three independent ES cell colonies were identified as correctly targeted (KO2, KO4, and KO6). All correctly targeted colonies appeared to be mixed clones containing targeted and WT alleles as revealed by external primers (F1-R2), and pure clones were generated by sub-cloning.

For $NLGN4^{R704C}$ a selection cassette containing an internal ribosomal entry site (IRES) and the Neomycin resistance gene (NEO) were used. For $NLGN4^{HA}$ the selection cassette was flanked by two flippase recognition target (FRT). For $NLGN4^{KO}$ and $NLGN4^{R704C}$ the selection cassette was flanked by two locus of X-over P1 (loxP). A point mutation was introduced into exon 7 and a floxed selection cassette into the 3′ intron of NLGN4. Ten clones were screened by PCR with external primers and four clones with correctly targeted $NLGN4^{R704C}$ alleles (KI4, KI6, KI7, and KI9) were identified. After transient expression of Cre recombinase, screening of clones by DNA sequencing using internal primers (F5-R5) led to the identification of sub-clones containing only the WT allele (clone KI4.1), the R704C allele (clone KI4.9) or still mixed sub-clones (containing both alleles as in KI4.7).

Electrophysiology

The iN cells were visualized using an X-cite 120Q fluorescence lamp (Lumen Dynamics) and an Olympus BX51WI microscope equipped with a Rolera-XR camera (Qimaging). Whole-cell patches were established at room temperature using MPC-200 manipulators (Sutter Instrument) and a Multiclamp 700B amplifier (Molecular Devices) controlled by Clampex 10 Data Acquisition Software (Molecular Devices). Pipettes were pulled using a PC-10 puller (Narishige) from borosilicate glass (o.d. 1.5 mm, i.d. 0.86 mm; Sutter Instrument) to a resistance of 2–3 MOhm and were filled with internal solution containing (in mM) 135 CsCl2, 10 HEPES, 1 EGTA, 1 Na-GTP, and 1 QX-314 (pH adjusted to 7.4, 310 mOsm). The bath solution contained (in mM) 140 NaCl, 5 KCl, 2 CaCl2, 1 MgCl2, 10 glucose, and 10 HEPES-NaOH (pH 7.4). An extracellular concentric bipolar electrode (FHC) was placed on the culture monolayer at a distance of approximately 80 μM from the recording cell. Evoked responses were induced by injecting a 1-ms, 1-mA current through an Isolated Pulse Stimulator 2100 (A-M Systems) connected to the stimulating electrode. For voltage-clamp experiments, the holding potential was −70 mV. The coefficient of variation for AMPAR-mediated evoked EPSCs was calculated

(SD/mean) from 5–10 consecutive trials. Pharmacological agents were used to confirm the presence of EPSCs and IPSCs in mixed cultures: picrotoxin (50 μM; Tocris) and 6-Cyano-7-nitroquinoxaline-2,3-3-dione (CNQX, 25 μM; Tocris). The mEPSC and mIPSC (but not the sEPSC and sIPSC) were recorded in the presence of TTX (a voltage-gated Na^+-channel blocker, 1 μM; Fisher Scientific). Only neurons with elaborate morphological complexity were selected for patching. For mEPSC/mIPSC and sEPSC/sIPSC experiments, only cells with at least 30 synaptic events were included in the analysis. For all experiments, the experimenter was blind to the recording condition. Experiments were performed in three different cultures replicates.

Rapid Autopsy

Human brain samples were harvest within 9 h after death from refrigerated bodies and flash frozen within one minute in liquid nitrogen.

Stochastic Optical Reconstruction Microscopy (STORM) Imaging:

dSTORM images were recorded with a Vutara SR 352 (Bruker Nanosurfaces, Inc., Madison, WI) commercial microscope based on single molecule localization biplane technology (Juette et al., 2008; Mlodzianoski et al., 2009). Cultures of induced neurons were labeled with primary antibodies as described above and secondary antibodies conjugated to Alexa647 (ThermoFisher) or CF568 (Biotium) and placed in dSTORM buffer containing (in mM) 50 Tris-HCl at pH 8.0, 10 NaCl, 20 MEA, 1% β-mercaptoethanol, 10% glucose, 150 AU glucose oxidase type VII (Sigma), and 1500 AU catalase (Sigma). Labeled proteins were imaged with 647nm and 561 nm excitation power of 16kW/cm^2. Images were recorded using a 60x/1.2 NA Olympus water immersion objective and Hamamatsu Flash4 V1 sCMOS camera with gain set at 50 and frame rate at 50 Hz. Data was analyzed by the Vutara SRX software (version 6.04). Single molecules were identified by their brightness frame by frame after removing the background. Identified molecules were localized in three dimensions by fitting the raw data in a 12x12-pixel region of interest centered around each particle in each plane with a 3D model function that was obtained from recorded bead datasets. Fit results were filtered by a density based denoising algorithm to remove isolated particles and rendered as 20 nm points. The experimentally achieved image resolution of 40 nm laterally (x,y) and 70 nm axially (in z) was determined by Fourier ring correlation.

QUANTIFICATION AND STATISTICAL ANALYSIS

All data are shown as means ± SEM of n = 3 where n is the number of independent biological replicates in all figure except in Figure 1B and S1C (human brain samples) where n is number of technical replicates. Numbers in bars represent number of cells/cultures analyzed, with statistical significance (* = $p < 0.05$, ** = $p < 0.01$ and *** = $p < 0.001$) determined by two-tailed Student's t test in GraphPad Prism. D'Agostino & Pearson omnibus normality test was used to determine normality for all datasets; all datasets were parametric.

DATA AND CODE AVAILABILITY

Raw sequencing data are deposited with the NCBI Gene Expression Omnibus under accession number GEO: GSE131428. Two biological replicates of FACS-sorted AM-iN cells, two biological replicates of Ngn2-iN cells and three biological replicates of AD-iN cells.

Raw data are available through Mendeley Data: https://doi.org/10.17632/g3wwzmrjv5.1. All software used is listed in the Key Resources Table.